Nonlinear Aerodynamic Modeling of Flap Oscillations in Transonic Flow: A Numerical Validation

W.J. Chyu* and L.B. Schiff†
NASA Ames Research Center, Moffett Field, California

The regime of validity of a nonlinear aerodynamic force and moment formulation, based on concepts from nonlinear functional analysis and applicable to a transonic airfoil with a deflecting flap, is investigated. A time-dependent finite difference technique is used to evaluate the aerodynamic data of the formulation in terms of specified, characteristic motions. Flap-motion histories are generated from the flap inertial equations of motion, with aerodynamic reactions specified by the moment formulation. The motion histories depicting the cases of decaying and growing flap oscillations are compared with histories generated through simultaneous, coupled solution of the fluid-dynamic equations and flap inertial equations of motion. The range of applicability of the formulation is discussed.

Nomenclature

a = speed of sound
c = chord length of airfoil plus undeflected flap
$C_h(t)$ = instantaneous flap hinge-moment coefficient, $h/q_\infty Sl$, Fig. 1
e = total energy per unit volume of fluid, normalized by $\rho_\infty a_\infty^2$
$\hat{E},\hat{F},\hat{q}$ = flux vectors of transformed gasdynamic equation, Eq. (2)
h = flap moment measured about hinge point, Fig. 1
I = flap moment of inertia
J = Jacobian of transformation between physical and computational coordinates
l = reference length, chosen equal to c, Eq. (1)
M = Mach number
p = pressure, normalized by $\rho_\infty a_\infty^2$
q_∞ = freestream dynamic pressure
S = reference area
t = time
u,v = Cartesian velocity components along the x,y axes, respectively, normalized by a_∞
U,V = contravariant velocity components, Eq. (4)
V_∞ = magnitude of freestream velocity vector
x,y = physical Cartesian coordinate axes, Fig. 1
α = angle of attack
ξ,η = computational coordinates in the axial and normal directions, respectively, Fig. 1
ρ = density, normalized by freestream density
σ_f = flap deflection angle, measured relative to chord line of airfoil, Fig. 1
τ = time, Eq. (2)
$(\dot{\ })$ = $\mathrm{d}/\mathrm{d}t(\ )$

I. Introduction

AIRCRAFT maneuvering at transonic speeds are subject to nonlinear, nonsteady aerodynamic loads on the airframe and control surfaces. Accurate means of predicting these nonlinear airloads are of great importance in analysis of the resulting flight motions and are needed in the design of flight control systems. Similarly, knowledge of the airloads is needed in the analysis of aeroelastic flutter boundaries. Prediction of nonsteady aerodynamic loads is complicated by the fact that the unsteady flowfield surrounding a maneuvering body, and thus the loading, is not determined solely by the instantaneous values of the motion variables, such as the angle of attack and control deflection angle. In general, the instantaneous state of the flowfield depends on the history of the flowfield, that is, on all the states taken during the course of the motion prior to the instant in question.

Recent papers have reported the results of unsteady flowfield computations for two-dimensional airfoils undergoing forced, or specified, harmonic oscillations in transonic flow. These computational methods were based on the unsteady inviscid Euler (e.g., Refs. 1-4) and potential (e.g., Refs. 5-9) gasdynamic equations and on the viscous Navier-Stokes[4] equations. Such computations yield the unsteady airloads on the body resulting from the specified motion. Although this information is very valuable, it does not entirely respond to the principal concern of the designer, which is to know the nature of the airloads for unspecified motions, that is, for the motions that may actually occur in flight. With the availability of the high-speed computer, it is now possible to consider responding directly to this concern by solving the flowfield equations *simultaneously* with the vehicle's inertial equations of motion for specified initial conditions. Results from these coupled computations would be complete time histories of airload responses and body motion, the latter specified in advance only insofar as the choice of initial conditions. Indeed, computations with this goal have already been carried out, based on the nonsteady Navier-Stokes equations, for the unconstrained motions of the flap on a two-dimensional airfoil at transonic speeds.[10] More recently, similar computations were carried out, based on the nonsteady potential equations, for an airfoil free to pitch about its midchord[11] and for the combined pitching and plunging motion of an elastically restrained airfoil with a deflecting flap.[12]

Although direct coupling of the flowfield equations to the vehicle inertial equations of motion in principle represents an exact approach to the problem of arbitrary maneuvers, one that automatically accounts for all time-history effects within the flowfield, it will inevitably be a very costly approach. This will be especially true when the aerodynamic loads are nonlinearly dependent on the motion variables. Under such conditions, the vehicle can experience widely differing motion histories, even if the initial conditions of the motions are close. Thus, to completely evaluate the vehicle's performance

Presented as Paper 81-0073 at the AIAA 19th Aerospace Sciences Meeting, St. Louis, Mo., Jan. 12-15, 1981; submitted April 8, 1981; revision received April 20, 1982. This paper is declared a work of the U.S. Government and therefore is in the public domain.

*Research Scientist, Aerodynamic Research Branch. Member AIAA.

†Research Scientist, Aerodynamic Research Branch. Associate Fellow AIAA.

envelope, a large number of coupled computations will be required, one for each change in initial conditions. Further, with the coupled-equations approach there can be no reutilization of the previously obtained aerodynamic results.

An alternative approach, in which a principal goal is to avoid the need for lengthy coupled computations, is to rely on mathematical modeling to describe the nonlinear aerodynamic terms (both steady and nonsteady) in the vehicle's equations of motion. In formulating a model, one tries to specify a *form* for the aerodynamic response that underlies the response to any given motion. Ideally such a model would require a determination of the aerodynamic terms only once; they would then be applicable (i.e., reusable) over a range of motion variables and flight conditions. Flight motions could then be predicted by solving the vehicle's equations of motion independently of the fluid-dynamic equations. In the case of linear aerodynamics, the modeling approach has led to the use of the related concepts of linear indicial responses and linear stability derivatives. In a series of papers (cf., Ref. 13 for a summary), Tobak and his colleagues showed how the indicial response and stability derivative concepts could be extended in a rational manner into the nonlinear aerodynamic regime. Their analysis suggests that the nonlinear aerodynamic response to an arbitrary motion of a body can be modeled from knowledge of the aerodynamic responses to a small number of specified characteristic motions.

In this paper we investigate the applicability of the nonlinear aerodynamic formulation to model the nonlinear, nonsteady aerodynamic forces on a two-dimensional airfoil with an oscillating flap at transonic speeds. The particular airfoil considered is an NACA 64A010 section hinged at 75% chord, at $M_\infty = 0.8$. Finite difference computations based on the nonsteady Euler equations are used to evaluate aerodynamic data in terms of the characteristic motions called for by the formulation. Histories of the flap motion are generated from the flap's inertial equations, with the aerodynamic reactions specified by the nonlinear aerodynamic formulation. These motion histories are compared with motion histories generated from solutions that are in principle exact, namely, simultaneous solutions of the Euler gasdynamic equations and the flap's equations of motion. The use of identical numerical techniques to evaluate the aerodynamic coefficients in terms of the characteristic motions in the modeling approach and also to generate motion histories using the coupled-equations approach ensures that the unsteady aerodynamic responses in both approaches are treated consistently. The applicability of the mathematical modeling approach in the nonlinear transonic regime is demonstrated by the close agreement between the motion histories obtained from the modeling approach and those obtained using the coupled-equations technique.

The form that the aerodynamic mathematical model takes and the resulting characteristic motions for the case of an oscillating flap are discussed in Sec. II. An overview of the numerical flowfield solution method is outlined in Sec. III, and results of flowfield computations for the aerodynamic data corresponding to the characteristic motions are presented in Sec. IV. Also presented in Sec. IV are histories of the flap deflection angle generated from both the aerodynamic formulation and the coupled-equations approach.

II. Aerodynamic Mathematical Model

Coordinate System and Notation

The two-dimensional airfoil and flap under consideration is an NACA 64A010 section hinged at the 75% chord point (Fig. 1). The x,y coordinate system is fixed to the airfoil with x aligned with the chord line. The forward portion of the airfoil remains at fixed inclination $\alpha = 0$ deg to the freestream. The flap, however, is free to execute a single-degree-of-freedom motion about its hinge point. The flap deflection angle σ_f is defined as positive for a downward displacement of the flap trailing edge. The hinge-moment coefficient C_h is measured about the flap hinge point. As shown in Fig. 1, a positive hinge-moment coefficient would tend to increase the flap deflection angle.

Nonlinear Moment Formulation

In a series of papers, Tobak and his colleagues have applied concepts from nonlinear functional analysis to derive a hierarchy of aerodynamic mathematical models allowing for a succession of increasingly complex aerodynamic phenomena (cf. Refs. 13 and 14). In general, the mathematical models are derived by 1) identifying the motion variables describing the motion under consideration, 2) defining the aerodynamic indicial responses to independent step changes in each of the motion variables, and 3) showing how the aerodynamic response to an arbitrary motion is obtained from a summation of the indicial responses. As discussed at length in Ref. 14, the level of complexity of the mathematical model is directly linked to the extent to which the indicial response is said to depend on the past history of the motion. The assumption that the aerodynamic indicial response is independent of the motion occurring prior to the step leads to the classical linear mathematical model. At the second level of approximation, the indicial response is assumed to depend solely on the state of the motion existent when the step is made. Mathematical models at this level of approximation are particularly suited to slowly varying motions and allow a rational introduction of nonlinear effects into the aerodynamic force and moment system. The assumption of slowly varying motions also allows one to reduce the formulation to a form correct to the first order in frequency. Aerodynamic mathematical models at this level have been derived to describe the general nonplanar flight motions of bodies of revolution and of aircraft.[13] When this level of approximation is applied to a treatment of the single-degree-of-freedom flap motion of interest, the resulting formulation for the instantaneous hinge-moment coefficient is

$$C_h(t) = C_h(\infty;\sigma_f(t)) + (\dot{\sigma}_f l/V_\infty) C_{h_{\dot{\sigma}_f}}(\sigma_f(t)) \qquad (1)$$

Consistent with the approximations made in its development, this formulation is valid for slowly varying motions of the flap, although the values of the flap deflection angle can be large. Each term in Eq. (1) is identified with a particular characteristic motion from which it can be evaluated. Thus the term $C_h(\infty;\sigma_f(t))$ is the hinge-moment coefficient that would be determined in a steady flow with the flap deflection angle held fixed at $\sigma_f(t)$. The remaining term, $C_{h_{\dot{\sigma}_f}}((\sigma_f(t))$, is the hinge-moment damping coefficient that would be evaluated for small-amplitude harmonic oscillations of the flap about a mean deflection angle held fixed at the instantaneous value $\sigma_f(t)$. These coefficient terms can be evaluated either through wind-tunnel tests or from the results of gasdynamic computations.

III. Numerical Technique

The time-dependent, inviscid Euler gasdynamic equations are solved to obtain the unsteady flowfield reactions to an arbitrary motion of the flap. The gasdynamic equations are solved using an implicit finite difference technique on a computational grid that conforms to the deforming airfoil.

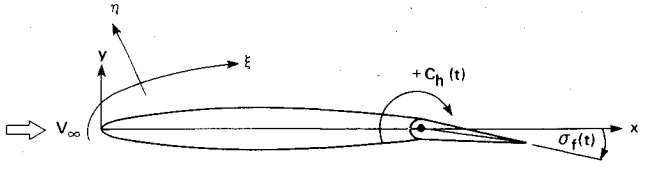

Fig. 1 Coordinates and notation.

Governing Gasdynamic Equations

The unsteady Euler equations can be written in strong conservation-law form for moving body-conforming coordinates ξ,η (Fig. 1) as

$$\partial_\tau \hat{q} + \partial_\xi \hat{E} + \partial_\eta \hat{F} = 0 \tag{2}$$

The flux vectors in Eq. (2) are

$$\hat{q} = J^{-1}\begin{bmatrix} \rho \\ \rho u \\ \rho v \\ e \end{bmatrix}, \quad \hat{E} = J^{-1}\begin{bmatrix} \rho U \\ \rho u U + \xi_x p \\ \rho v U + \xi_y p \\ (e+p)U - \xi_t p \end{bmatrix}$$

$$\hat{F} = J^{-1}\begin{bmatrix} \rho V \\ \rho u V + \eta_x p \\ \rho v V + \eta_y p \\ (e+p)V - \eta_t p \end{bmatrix} \tag{3}$$

The contravariant velocity components are defined in terms of the Cartesian velocities as

$$U = \xi_t + \xi_x u + \xi_y v, \quad V = \eta_t + \eta_x u + \eta_y v \tag{4}$$

The mapping between the x,y physical plane and the ξ,η computational plane is reflected in Eq. (2) through the presence of the metric terms $\xi_t,\xi_x,\xi_y,\eta_t,\eta_x,\eta_y$ and the Jacobian term $J=(\xi_x\eta_y-\xi_y\eta_x)$, which appear in the flux vectors. The metric and Jacobian terms are determined numerically once the instantaneous x,y coordinates of the grid points within the computational mesh have been specified.

Equation (2) is solved, subject to appropriate body and freestream boundary conditions, using an implicit finite difference method.[2] The method is noniterative, fully implicit, and is of second-order accuracy in both time and space.

Grid Generation

Computational grids are first constructed for the extreme positive and negative values of the flap deflection angle $\sigma_f = \pm 20$ deg (Fig. 2). Grids required at intermediate flap deflections are obtained from those at the extreme positions by spatial interpolation.

The extreme-position grids are generated by numerically solving a nonlinear Poisson equation.[15,16] This technique permits grid points to be specified along the outer boundaries of the computational region, that is, along the airfoil surface, the wake, and the freestream boundary. Applying the method then generates a smoothly spaced, non-overlapping grid at the interior points.

In the present work, boundary points are specified at fixed locations along the airfoil and flap surface ($\eta = 0$) with the flap in its neutral position, $\sigma_f = 0$. The surface points are clustered near the leading and trailing edges of the airfoil and near the flap hinge point. These surface boundary-point locations are retained for the stationary grids generated with the flap at its extreme deflections, $\sigma_f = \pm 20$ deg. With the flap at an extreme deflection, however, the surface grid spacing behind the hinge point becomes too congested on one side of the airfoil and too sparse on the opposite side. This undesirable tendency is eliminated by respacing the two surface grid points directly behind the hinge point along the flap surface as the flap is deflected.

The grid boundary points on the $\eta = 0$ line behind the flap trailing edge are chosen to lie on a parabolic arc tangent to the flap at its trailing edge and returning to the airfoil centerline at the rear of the computational grid. This procedure aligns the grid points in the wake with the approximate initial direction of the wake flow, and was found to improve the accuracy of the flowfield computations. Finally, grid points at the freestream boundary are chosen to lie approximately eight chord lengths above and below the airfoil and eight chords upstream and downstream from the airfoil leading edge. The outer boundary points remain fixed in space for all flap deflection angles.

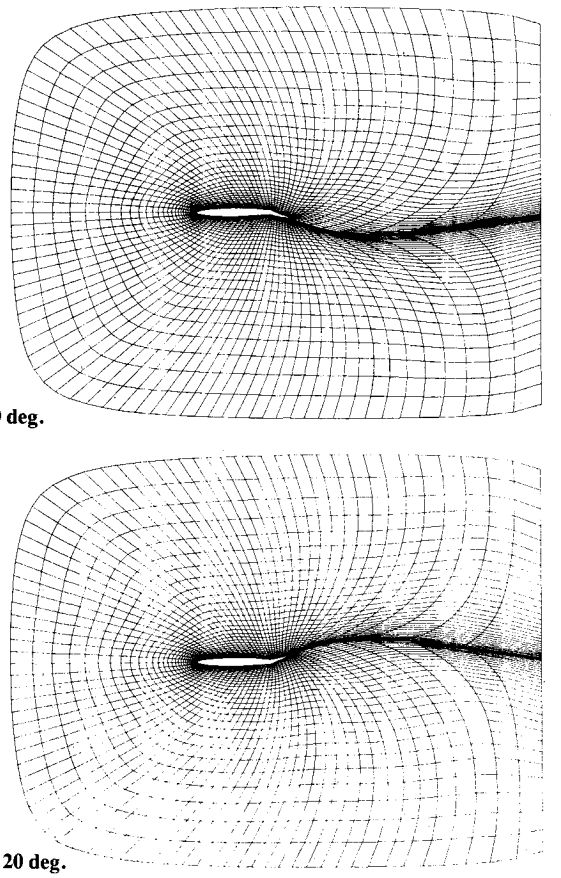

a) $\sigma_f = 20$ deg.

b) $\sigma_f = -20$ deg.

Fig. 2 Computational grids with flap at extreme deflections.

Once the grid is specified on the boundaries, the Poisson equation solver is used to generate a smoothly spaced grid at the interior points. This grid is then respaced, or clustered, along $\xi = \text{const}$ lines (lines moving away from the airfoil) using a weighted coordinate stretching technique.[4] The resulting grids for $\sigma_f = \pm 20$ deg are shown in Fig. 2; they demonstrate a fine spacing of the grid at the airfoil and a well-controlled grid spacing throughout the computational region.

As the airfoil flap undergoes movement during the flowfield computations, a new grid must be generated at each time-step of the computation. To reduce the computational effort that would be required to repeatedly generate grids using the Poisson equation technique, an interpolation scheme[4] is employed. The instantaneous unsteady grids at intermediate flap deflection angles are obtained by interpolating between the grids generated with the flap at its extreme deflections. The two surface grid points directly behind the hinge point are excluded from the interpolation, however, and are equally spaced between the newly interpolated adjacent surface points. After the instantaneous grid is determined, the metric quantities for that grid are obtained numerically.

Boundary Conditions

The boundary-conforming transformation maps the airfoil surface and the outer edge of the computational domain into $\eta = \text{const}$ lines. The condition of flow tangency along the airfoil is satisfied by setting the contravariant velocity $V = 0$ at the airfoil surface. The resulting Cartesian velocity com-

ponents are given on the surface in terms of the contravariant components as

$$\begin{bmatrix} u \\ v \end{bmatrix} = J^{-1} \begin{bmatrix} \eta_y & -\xi_y \\ -\eta_x & \xi_x \end{bmatrix} \begin{bmatrix} U-\xi_t \\ -\eta_t \end{bmatrix} \tag{5}$$

In applying Eq. (5), U is determined at the airfoil surface by a linear extrapolation from the flowfield determined at the previous time step, and

$$\xi_t = -x_\tau \xi_x - y_\tau \xi_y, \quad \eta_t = -x_\tau \eta_x - y_\tau \eta_y \tag{6}$$

where x_τ and y_τ are local surface velocities. In addition, the Kutta condition is applied at the flap trailing edge by setting u and v to x_τ and y_τ, respectively ($U=0$, $V=0$). Freestream conditions are maintained at the fixed outermost top, bottom, and upstream boundaries of the computational domain, and a simple extrapolation exit condition is applied at the downstream boundary.

IV. Results

Flowfield Computations for Characteristic Motions

Flowfield solutions were obtained for the airfoil and flap to determine the steady and nonsteady flap hinge-moment coefficients due to the flap motion. Computations were performed with fixed flap deflection angles ranging from 0 to 20 deg to evaluate the static hinge-moment coefficient $C_h(\infty;\sigma_f)$. To determine the flap hinge-moment damping coefficient $C_{h_{\dot{\sigma}_f}}(\sigma_f)$, computations were performed for specified small-amplitude harmonic oscillations of the flap about mean flap deflections ranging from 0 to 20 deg. In all cases, the Mach number was held fixed at $M=0.8$ and the airfoil angle of attack was held fixed at $\alpha=0$ deg.

Code Performance

The computations were carried out on a grid having 87 points in the ξ direction and 41 points in the η direction. The airfoil was defined by 61 points in the ξ direction, and the remainder of the ξ points lay along the wake. Computation time on a CDC 7600 computer was 3.1 s/time-step with this size grid. For steady flow, the computations typically required 500 time-steps to obtain a converged solution.

For nonsteady flow, computations were initiated using previously obtained steady solutions. The flap was specified to move sinusoidally with instantaneous deflection angle

$$\sigma_f(t) = \sigma_{f_m} + \sigma_{f_l} \sin\omega t \tag{7}$$

where σ_{f_m} ranged from 0 to 20 deg and σ_{f_l} was small, usually equal to 0.5 deg. The reduced frequency $k=\omega l/V$ was held fixed at 0.15. A steady solution, obtained for $\sigma_f=\sigma_{f_m}$, was imposed as an initial solution, and computations were carried out for three cycles of flap motion, $0\le\omega t\le 6\pi$. Three cycles of oscillation were found to allow sufficient time for successive cycles of the response to the motion to become close enough to be called periodic. Throughout the computations the solution obtained for the third cycle of oscillation was indistinguishable from that obtained in response to the second cycle. Each cycle of the harmonic flap motion required 1200 time-steps.

Steady Flow

Surface-pressure coefficient distributions on the airfoil and flap, obtained from the computations for steady flow, are shown in Fig. 3 for the various flap deflection angles. Mach number contour distributions corresponding to several of these flap deflections are shown in Fig. 4. At $\sigma_f=0$ deg (Fig. 3) a shock wave is observed at $x/c=0.5$ on both the upper and lower surfaces of the airfoil. As the flap deflection increases, the shock on the upper surface is located farther aft on the airfoil. The region of supersonic flow (indicated in Fig. 4 by

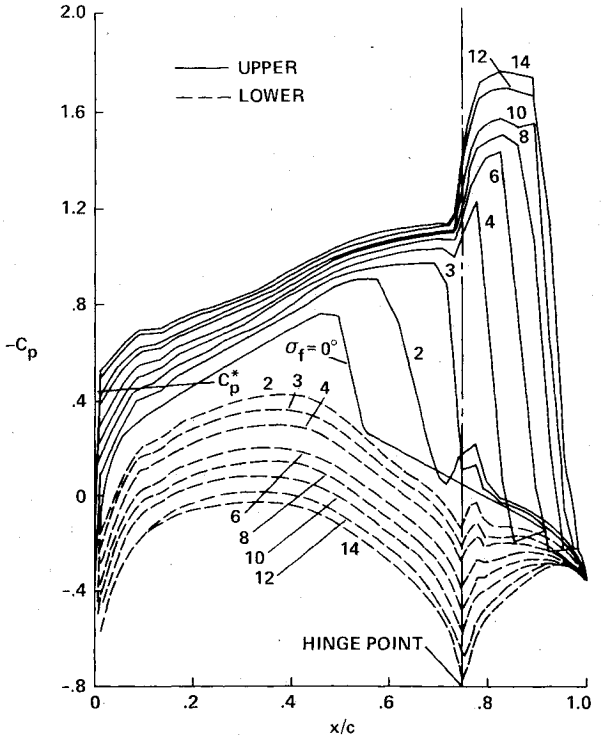

Fig. 3 Static surface-pressure distributions; $M_\infty=0.8$.

the $M=1.0$ contour) becomes larger, and the shock strength is increased. At $\sigma_f=3$ deg (Fig. 4b) the upper-surface shock wave has moved to the flap hinge point. Further increases in flap deflection cause the shock to move aft along the flap surface (Figs. 4c-e). As the flap deflection increases beyond $\sigma_f=10$ deg, the shock wave is located essentially at the flap trailing edge (Fig. 3).

The steady surface-pressure distributions were spatially integrated to obtain the flap static hinge-moment coefficient $C_h(\infty;\sigma_f)$. These results are presented in Fig. 5 as a function of the flap deflection angle. The hinge-moment coefficient is a linear function of σ_f for $|\sigma_f|<3$ deg and is always statically stable, tending to oppose the flap deflection. For flap deflections greater than $\sigma_f=3$ deg, where the shock wave on the upper surface moves onto the flap, the hinge-moment coefficient is a nonlinear function of the deflection angle.

Nonsteady Flow

Time histories of the hinge-moment coefficient, obtained from small-amplitude harmonic oscillations of the flap about fixed mean values of the flap deflection angle σ_{f_m}, are shown in Fig. 6. The moment time histories are obtained from spatial integration of the instantaneous surface-pressure coefficient distributions. The results demonstrate a mild time variation of the moment coefficient for mean flap deflection angles less than 3 deg, where the shock wave on the upper surface lies forward of the flap hinge point. For mean flap angles between 3 and 10 deg, the moment time histories exhibit a greater sensitivity to the flap motion. The large amplitude of the response is due mainly to the movement of the shock wave along the flap during the course of the motion. With further increases in σ_{f_m} above 10 deg, the shock wave position changes only slightly, although the strength of the shock does increase. Thus for $\sigma_{f_m}>10$ deg the hinge-moment coefficient again exhibits a mild time variation.

The flap hinge-moment damping coefficient $C_{h_{\dot{\sigma}_f}}(\sigma_f)$ is evaluated from the component of the hinge-moment coefficient time history that is 90 deg out of phase with the time history of the flap deflection angle. These results are presented in Fig. 7 as a function of the mean flap deflection

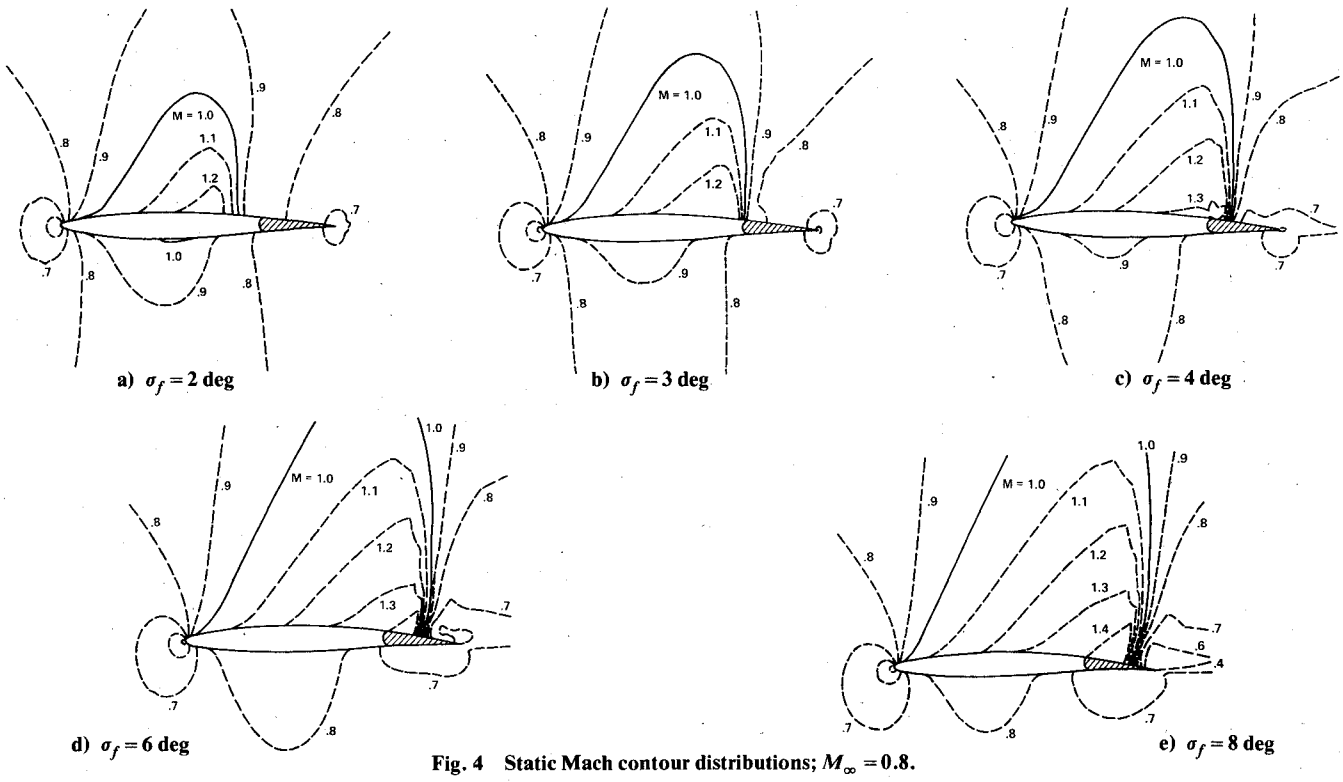

a) $\sigma_f = 2$ deg b) $\sigma_f = 3$ deg c) $\sigma_f = 4$ deg

d) $\sigma_f = 6$ deg e) $\sigma_f = 8$ deg

Fig. 4 Static Mach contour distributions; $M_\infty = 0.8$.

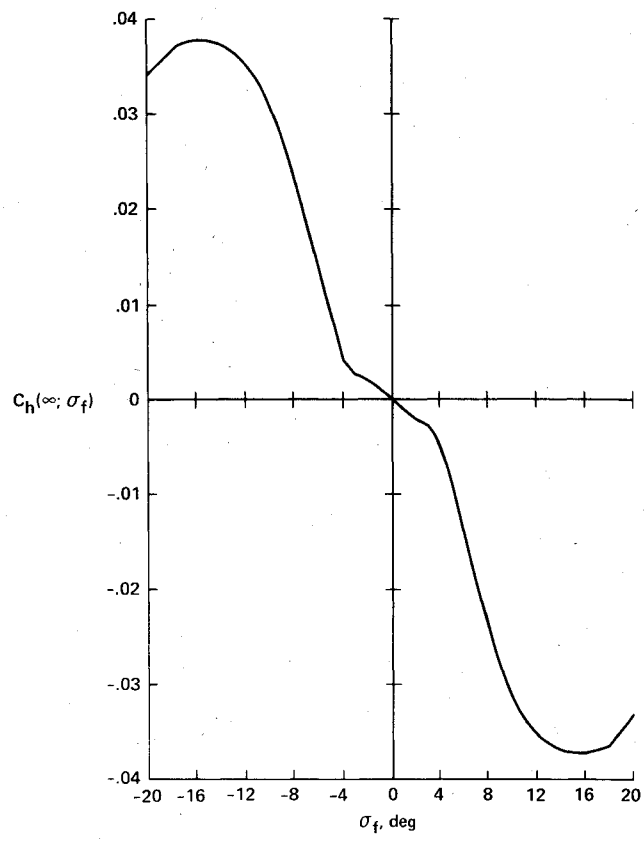

Fig. 5 Static hinge-moment coefficient; $M_\infty = 0.8$.

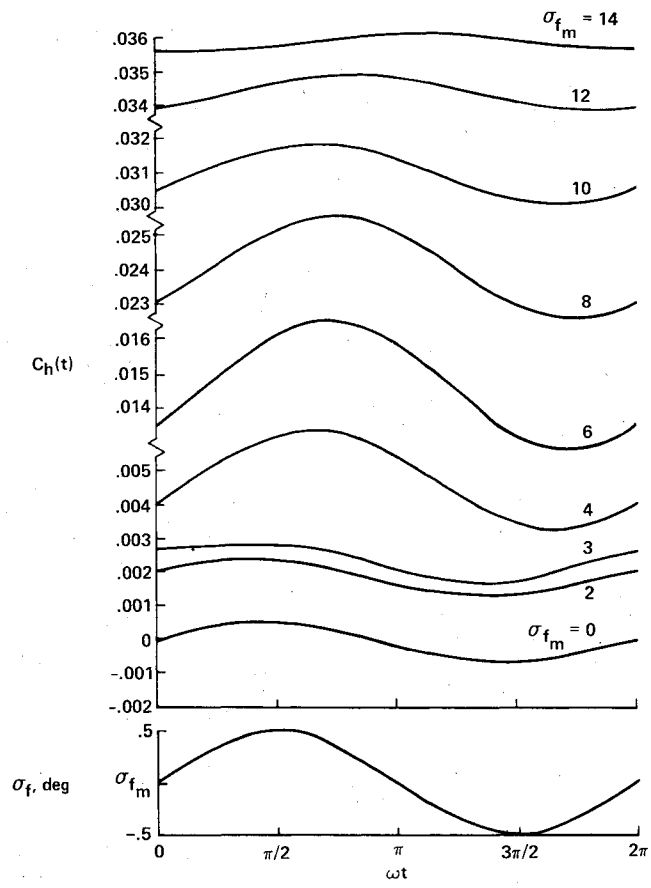

Fig. 6 Time histories of hinge-moment coefficient response to forced oscillation; $\sigma_f(t) = \sigma_{f_m} + \sigma_{f_1} \sin\omega t$, $\sigma_{f_1} = 0.5$ deg.

angle. At the flow conditions investigated, the flap damping coefficient is a highly nonlinear function of the flap attitude. For values of $|\sigma_{f_m}| < 3$ deg, the damping coefficient is negative and would tend to damp an unconstrained oscillation of the flap. For values of σ_{f_m} ranging between 3 and 17 deg, however, the flap damping coefficient is positive and would cause an unconstrained oscillation of the flap to grow in amplitude (dynamically destabilizing).

The destabilizing trend in the flap hinge-moment damping coefficient is, of course, due to the detailed pressure distributions that occur on the flap. Some insight into this destabilizing trend can be obtained by showing its qualitative linkage to the slope of the static hinge-moment coefficient. To establish this insight, let us first consider the trend of the aero-

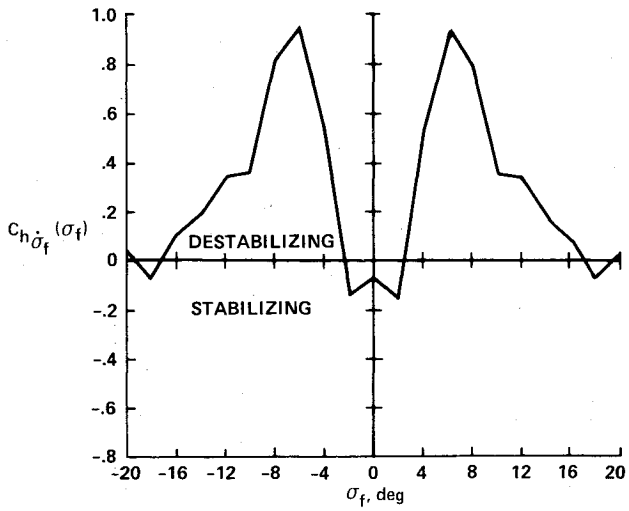

Fig. 7 Hinge-moment damping coefficient; $M_\infty = 0.8$.

dynamic damping-in-pitch coefficient $\{C_{m_q}(\infty;\alpha) + C_{m_{\dot{\alpha}}}(\alpha)\}$ that would be measured for an airfoil performing small-amplitude harmonic oscillations in angle of attack about a mean angle of attack α. It is known that the contribution of $C_{m_q}(\infty;\alpha)$ to the airfoil damping is always stabilizing, whereas that of $C_{m_{\dot{\alpha}}}(\alpha)$ can be destabilizing. Further, it can be shown (cf. Ref. 13) that a simple qualitative relationship exists between $C_{m_{\dot{\alpha}}}$ and the static aerodynamic pitching-moment coefficient, namely,

$$C_{m_{\dot{\alpha}}}(\alpha) = A + BC_{m_\alpha}(\infty;\alpha) \tag{8}$$

where A and B are constants (with $B<0$) and $C_{m_\alpha}(\infty;\alpha)$ is the local slope of the static pitching-moment curve. Thus, at angles of attack where C_{m_α} is large and negative, $C_{m_{\dot{\alpha}}}(\alpha)$ will be correspondingly large and positive and will tend to make $\{C_{m_q}(\infty;\alpha) + C_{m_{\dot{\alpha}}}(\alpha)\}$ destabilizing. A completely analogous trend is observed for the case of the oscillating flap. In the region of flap deflection angle where the slope of $C_h(\infty;\sigma_f)$ is small, $\sigma_{f_m} < 3$ deg, $C_{h_{\dot{\sigma}_f}}(\sigma_f)$ is stabilizing. At slightly larger deflections, 3 deg $< \sigma_{f_m} <$ 9 deg, the negative slope of the static hinge-moment curve increases sharply and $C_{h_{\dot{\sigma}_f}}(\sigma_f)$ becomes destabilizing. As the flap deflection angle increases beyond $\sigma_{f_m} = 9$ deg, the negative slope of the static curve decreases to zero ($\sigma_{f_m} = 16$ deg) and becomes positive, while $C_{h_{\ddot{\sigma}_f}}(\sigma_f)$ again tends toward stabilizing values.

Flap-Motion Histories

The inertial equation governing mechanically unconstrained motions of the flap is

$$I\ddot{\sigma}_f(t) = qSlC_h(t) \tag{9}$$

Flap-motion histories were generated by time integration of Eq. (9), for various initial conditions, with the instantaneous hinge-moment coefficient determined from both the coupled-equations technique and the aerodynamic mathematical model approach.

Coupled-Equations Technique

Baseline flap-motion histories were generated by solving the inertial equation [Eq. (9)] simultaneously with the Euler gasdynamic equations [Eq. (2)]. Coupling of the inertial equation with the gasdynamic equations is conceptually a straightforward numerical procedure. At each time step in the solution of the gasdynamic equations, the instantaneous metric terms $\xi_x, \xi_y, \eta_x, \eta_y$ and their time variations ξ_t and η_t must be supplied to the computation. In nonsteady computations that determine the aerodynamic response to a prespecified motion, the metric terms and their time variation are known in advance for all times during the interval of the computation. In contrast, using the coupled-equations approach, the flap position, the flap velocity, and the value of the instantaneous hinge-moment coefficient are known only at an initial time. To advance the solution to the next time level, Eq. (9) is used to predict the new flap velocity and position, thus determining new values of the metric terms. These new metric terms, along with updated values of their time variations, are entered into the gasdynamic computation to determine the instantaneous state of the flowfield and the instantaneous hinge-moment coefficient at the new time level. After determination of the flap position and hinge-moment coefficient at the new time level, this procedure is repeated to generate both the flap-motion history and the time history of the aerodynamic response. Coupling of the gasdynamic and inertial equations in this manner automatically includes, in principle, proper consideration of all nonsteady and nonlinear effects.

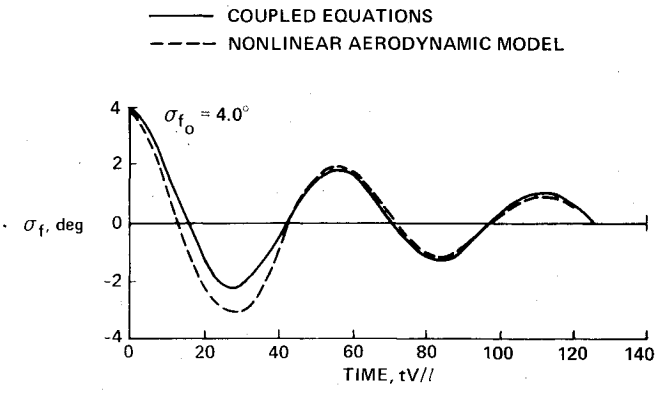

Fig. 8 Time history of flap deflection; $\sigma_{f_0} = 4.0$ deg.

Aerodynamic Mathematical Model Approach

Histories of the flap motion were also generated from the flap inertial equation, with the instantaneous hinge-moment coefficient specified by the nonlinear aerodynamic mathematical model, Eq. (1). Upon specifying initial values of the flap deflection angle and flap velocity, Eq. (9) was integrated numerically, using an Adams predictor-corrector method, to generate flap-motion histories. At each time level in the solution, the flap velocity and deflection are known. The instantaneous hinge moment is given by Eq. (1), where the terms $C_h(\infty;\sigma_f(t))$ and $C_{h_{\dot{\sigma}_f}}(\sigma_f(t))$ are obtained from table look-ups in Figs. 5 and 7, respectively.

Comparison of Motion Histories

Oscillatory histories of the flap motion, generated with both the coupled-equations technique and the mathematical modeling approach for the case where the flap was released from rest with an initial deflection $\sigma_{f_0} = 4.0$ deg, are shown in Fig. 8. The stabilizing portion of the damping curve (Fig. 7) controls the motion, and the oscillation amplitude decays smoothly. In this case the flap moment of inertia was chosen to give a value of reduced frequency close to the one specified for the forced-oscillation gasdynamic computations. This procedure eliminated any higher-order frequency effects. When the flap is released from a slightly larger initial attitude, $\sigma_{f_0} = 4.5$ deg, the destabilizing region of the damping coefficient curve causes the amplitude of the resulting oscillatory motion to grow rapidly (Fig. 9). In both cases the motions generated using the nonlinear mathematical model agree well with the baseline motion histories, thus demonstrating the validity of the model. In contrast, a motion history generated for the $\sigma_{f_0} = 4.5$ deg case using a mathematical model that does not account for nonlinear, nonsteady effects [i.e., Eq. (1) with a nonlinear variation of the static aerodynamic term

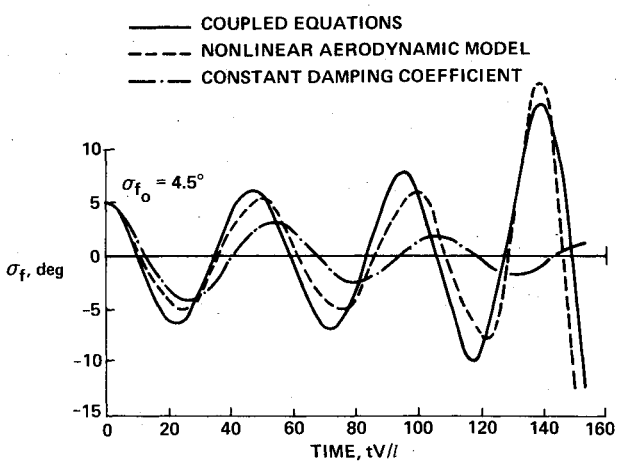

Fig. 9 Time history of flap deflection; $\sigma_{f_0} = 4.5$ deg.

and with the value of the damping term $C_{h_{\dot{\sigma}_f}}$ held fixed for all σ_f at the value obtained at $\sigma_f = 0$ deg] completely fails to predict the undamped growth.

V. Discussion

The demonstrated ability of the aerodynamic formulation to model the nonlinear, nonsteady aerodynamics acting in this example has important implications for the treatment of future problems involving nonsteady motions. In our opinion, the mathematical modeling approach has the significant advantages of lower costs and greater physical insight than the approach requiring solutions of the coupled inertial and gasdynamic equations.

First, with respect to costs, if large numbers of motion histories need to be calculated, the modeling approach will be less expensive than the coupled-equations approach. Once the initial costs of evaluating the aerodynamic coefficients in terms of the characteristic motions are expended, computation of the single-degree-of-freedom motion histories requires a relatively insignificant additional expense. In the present example, 11 characteristic-motion computations were carried out for mean flap deflections spaced every 2 deg ranging from $\sigma_f = 0$ to 20 deg. Each of the coupled-equations computations, on the other hand, required computer costs approximately equal to the costs of one of the characteristic-motion computations. Thus in this instance, if more than 11 coupled cases were to be evaluated, the modeling approach would be less costly. Moreover, the modeling approach makes it easy to introduce changes into Eq. (9) (for example, changing the flap moment of inertia or center-of-mass location, adding mechanical damping, or adding a restoring force) and to evaluate their effects at low cost, since the aerodynamic data in the mathematical model would remain the same. By contrast, in the coupled-equations approach, the simplest change in any of the equations would require a complete re-evaluation of the flowfield and flap response.

Second, the modeling approach gives better insight into the physics governing the unsteady flow than does the coupled-equations approach. If an undamped or divergent motion results from computations based on the coupled-equations approach, one knows little more than the fact that it occurs. Computations carried out in terms of the characteristic motions allow an investigation into the physical mechanisms underlying the resulting unconstrained motions. In the present case, the computations for steady flow indicated that it was the rearward movement of the shock wave onto the flap that caused the large negative increase in the slope of the static hinge-moment coefficient curve. Further, it was possible to determine how the change in the static hinge-moment coefficient was related to the destabilizing behavior of the hinge-moment damping coefficient. Also, in this case, knowledge of the behavior of the damping coefficient with increasing deflection angle allowed us to qualitatively predict the types of flap-motion histories that were later computed.

The aerodynamic mathematical model validated in this paper is one of a hierarchy of mathematical models that allow for a succession of increasingly complex aerodynamic phenomena. Under certain flow conditions the mathematical model, as presented in Eq. (1), will no longer be valid. The lack of applicability of the model will become apparent when the assumptions contained within the aerodynamic model are not consistent with the results of the characteristic-motion computations. Specifically, as a result of the assumptions made in obtaining the model, the nonsteady aerodynamic term in Eq. (1), although a nonlinear function of flap deflection, varies linearly with the reduced frequency. In the event that the computational results for the aerodynamic reactions to a characteristic motion are found to violate the assumptions of the aerodynamic formulation (i.e., in this example, to vary nonlinearly with frequency), then the mathematical model at the next level of complexity would have to be adopted. (See Refs. 13 and 14 for a full discussion.) The aerodynamic data would then be determined in terms of the characteristic motions called for by the new formulation. In this manner a mathematical model can be systematically selected at the lowest level of complexity needed to account for the aerodynamic phenomena (e.g., hysteresis, dynamic stall) that the vehicle is found to experience.

VI. Concluding Remarks

The regime of validity of an aerodynamic mathematical model, applicable to the nonlinear aerodynamic reactions on a transonic airfoil with a deflecting flap, has been investigated. A time-dependent finite difference technique was used to compute the nonsteady flowfields, and thus to determine the nonlinear, nonsteady aerodynamic data required by the model, in terms of specified characteristic motions. Flap-motion histories were generated from the flap inertial equations of motion with the aerodynamic reactions specified through use of the mathematical model. These were compared with baseline flap-motion histories obtained from simultaneous, coupled solutions of the gasdynamic and inertial equations. The flap-motion histories generated with the aerodynamic mathematical model approach agreed well with those obtained from the coupled-equations approach, even for a case in which the flap exhibited an undamped oscillatory behavior.

Acknowledgment

The authors are grateful to Murray Tobak for his valuable comments and suggestions during the course of this study.

References

[1] Magnus, R. and Yoshihara, H., "Unsteady Flows over an Airfoil," *AIAA Journal,* Vol. 13, Dec. 1975, pp. 1622-1628.

[2] Steger, J.L., "Implicit Finite-Difference Simulation of Flow About Arbitrary Two-Dimensional Geometries," *AIAA Journal,* Vol. 16, July 1978, pp. 679-686.

[3] Lerat, A. and Sides, J., "Numerical Calculations of Unsteady Transonic Flows," AGARD CP-226, *Unsteady Airloads in Separated and Transonic Flow*, Paper 14, April 1977, pp. 14-1 to 14-11.

[4] Chyu, W.J., Davis, S.S., and Chang, K.S., "Calculation of Unsteady Transonic Flow over an Airfoil," *AIAA Journal,* Vol. 19, June 1981, pp. 684-690.

[5] Ballhaus, W.F. and Goorjian, P.M., "Implicit Finite Difference Computations of Unsteady Transonic Flows About Airfoils," *AIAA Journal*, Vol. 15,Dec. 1977, pp. 1728-1735.

[6] Rizzetta, D.P. and Chin, W.C., "Effect of Frequency in Unsteady Transonic Flow," *AIAA Journal,* Vol. 17, July 1979, pp. 779-781.

[7] Rizzetta, D.P. and Yoshihara, H., "Computation of the Pitching Oscillation of an NACA 64A010 Airfoil in the Small Disturbance Limit," AIAA Paper 80-0128, 1980.

[8] Isogai, K., "Calculation of Unsteady Transonic Flow Using the Full Potential Equation," AIAA Paper 77-448, 1977.

[9]Goorjian, P.M., "Implicit Computation of Unsteady Transonic Flow Governed by the Full Potential Equation in Conservation Form," AIAA Paper 80-0150, 1980.

[10]Steger, J.L. and Bailey, H.E., "Calculation of Transonic Aileron Buzz," *AIAA Journal,* Vol. 18, March 1980, pp. 249-255.

[11]Ballhaus, W.F. and Goorjian, P.M., "Computation of Unsteady Transonic Flows by the Indicial Method," *AIAA Journal,* Vol. 16, Feb. 1978, pp. 117-124.

[12]Rizzetta, D.P., "Time-Dependent Response of a Two-Dimensional Airfoil in Transonic Flow," *AIAA Journal,* Vol. 17, Jan. 1979, pp. 26-32.

[13]Tobak, M. and Schiff, L.B., "On the Formulation of the Aerodynamic Characteristics in Aircraft Dynamics," NASA TR R-456, Jan. 1976.

[14]Tobak, M. and Schiff, L.B., "The Role of Time-History Effects in the Formulation of the Aerodynamics of Aircraft Dynamics," AGARD CP-235, *Dynamic Stability Parameters,* Paper 26, May 1978, pp. 26-1 to 26-10.

[15]Thompson, J.F., Thames, F.C., and Mastin, C.W., "Automatic Numerical Generation of Body-Fitted Curvilinear Coordinate System for Field Containing Any Number of Arbitrary Two-Dimensional Bodies," *Journal of Computational Physics,* Vol. 15, July 1974, pp. 299-319.

[16]Sorensen, R.L. and Steger, J.L., "Simplified Clustering of Nonorthogonal Grids Generated by Elliptic Partial Differential Equations," NASA TM-73252, Aug. 1977.